The role of axis embedding on rigid rotor decomposition analysis of variational rovibrational wave functions

Tamás Szidarovszky, Csaba Fábri, and Attila G. Császár

Additional information on J. Chem. Phys.
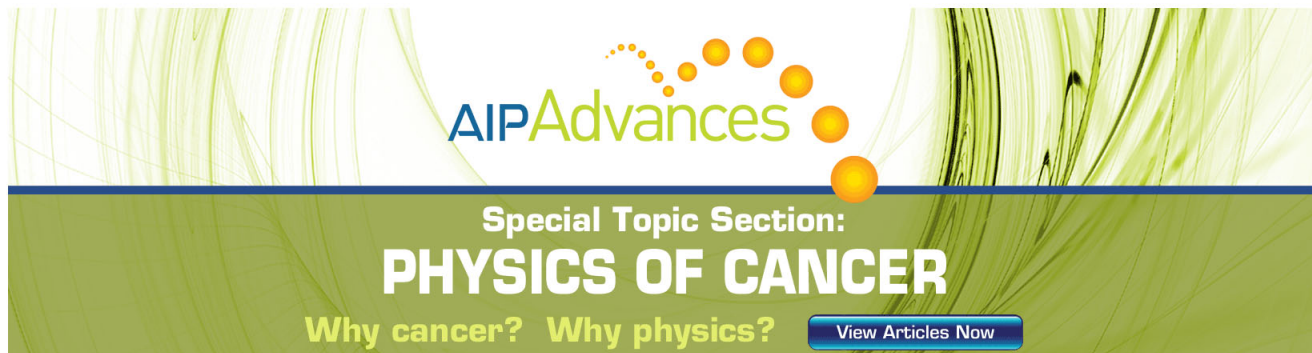
The role of axis embedding on rigid rotor decomposition analysis of variational rovibrational wave functions

Tamás Szidarovszky, Csaba Fábri, and Attila G. Császár
Laboratory of Molecular Structure and Dynamics, Institute of Chemistry, Eötvös University, H-1117 Budapest, Pázmány Péter sétány 1/A, Hungary

Approximate rotational characterization of variational rovibrational wave functions via the rigid rotor decomposition (RRD) protocol is developed for Hamiltonians based on arbitrary sets of internal coordinates and axis embeddings. An efficient and general procedure is given that allows employing the Eckart embedding with arbitrary polyatomic Hamiltonians through a fully numerical approach. RRD tables formed by projecting rotational-vibrational wave functions into products of rigid-rotor basis functions and previously determined vibrational eigenstates yield rigid-rotor labels for rovibrational eigenstates by selecting the largest overlap. Embedding-dependent RRD analyses are performed, up to high energies and rotational excitations, for the $H_2{}^{16}O$ isotopologue of the water molecule. Irrespective of the embedding chosen, the RRD procedure proves effective in providing unambiguous rotational assignments at low energies and J values. Rotational labeling of rovibrational states of $H_2{}^{16}O$ proves to be increasingly difficult beyond about 10 000 cm^{-1}, close to the barrier to linearity of the water molecule. For medium energies and excitations the Eckart embedding yields the largest RRD coefficients, thus providing the largest number of unambiguous rotational labels. © 2012 American Institute of Physics. [http://dx.doi.org/10.1063/1.4707463]

I. INTRODUCTION

Molecular spectra have been studied at high resolution extensively as accurate knowledge of rovibronic data is needed in a large number of scientific and engineering applications.[1,2] Experiments provide accurate but highly incomplete information, as shown, for instance, on the example of the relatively thoroughly studied isotopologues of the water molecule.[3,4] Variational quantum chemical techniques[2,5–9] have been developed and applied to molecules containing a "few" atoms to study their rotation-vibration states up to[10] and even beyond[11,12] the first dissociation limit for a given potential energy surface (PES). One of the results of a variational solution of the nuclear Schrödinger equation is a set of rovibrational eigenvalues, from which transition wavenumbers and thus positions in a high-resolution spectrum can be deduced. Another set of results comes in the form of rovibrational eigenfunctions, underlying transition intensities and line shapes. A variational nuclear motion computation of spectroscopic significance is not complete without characterization of the eigenstates of the molecule, usually in form of exact and/or approximate quantum numbers attached to the eigenstates. It is this last task which is the subject of the present investigation.

There are several techniques developed to provide a qualitative understanding of the characteristics of the computed eigenvalues and eigenstates. The perhaps simplest and most traditional technique involves an energy decomposition scheme, employing the energy dependence of the vibrationally computed eigenenergies based on the normal mode quantum numbers and the knowledge of the vibrational fundamentals. Above a certain, usually rather low, energy threshold, the density of rovibrational states increases considerably

and there are often several candidates for a given set of vibrational normal mode quantum numbers making the assignment via this scheme impossible or at least dubious. Furthermore, as the wavefunction-based normal mode decomposition (NMD) analysis[8,13,14] showed, even when normal-mode labels can be allocated based on this scheme, their physical relevance can clearly be questioned. Second, inspection of 2D cuts of the real wave function plots along appropriately chosen coordinates sometimes gives valuable qualitative information on the molecular state.[10] However, these plots cannot be used to get quantitative information on states of heavy mixtures of basis states without significant manipulation,[15] which is rarely attempted. It would also be hard to identify multiply excited levels by visual inspection even if such a state was fairly harmonic. Third, certain expectation values of physical quantities related to the molecule studied can be computed resulting in approximate quantum numbers for each vibrational level. Normal-mode-like labels can also be created this way.[10] Fourth, perturbing certain cuts along the PES helps in the assignment of vibrational quantum numbers to levels with large quantum numbers associated with that coordinate. Changes in an eigenstate's energy is often found to be practically independent of the other quantum numbers, facilitating the assignment procedure.

Notwithstanding these possibilities, the most sound approach to assigning approximate quantum numbers to variationally computed wave functions must employ overlaps of the exact wave function with approximate model wave functions characterized by certain well-defined quantum numbers, perhaps exact for the models. This procedure is especially relevant, straightforward, and useful for spectroscopic applications when the model corresponds to the rigid rotor and harmonic oscillator approximations and the

associated functions. Such a procedure was developed in Ref. 13 for the Eckart–Watson Hamiltonian,[16,17] and was named NMD for vibrations and rigid rotor decomposition (RRD) for rotations. The Eckart–Watson Hamiltonian, however, can rarely be employed for large-amplitude motions and for nonrigid molecules. Energy levels and wave functions for such molecules must be computed with variational procedures based on Hamiltonians employing internal coordinates. One particularly appealing choice for *triatomic* molecular systems is the use of the Sutcliffe–Tennyson Hamiltonian.[18] A complementary approach with an exact kinetic energy operator (KEO) is provided by the GENIUSH (general nuclear motion code with numerical, internal-coordinate, user-specified Hamiltonians) protocol[19,20] having the following main characteristics: (a) it is applicable to *all* molecular systems of feasible size, irrespective of the fact whether their PESs contain a single minimum or multiple minima and what choice is made for the internal coordinates and the coordinate system embedding; (b) the exact analytical form of the KEO does not need to be known *a priori* as the KEO is constructed fully numerically; and (c) it allows the use of arbitrary reduced-dimensional nuclear motion treatments within the same code. Due to the well-known features of the Eckart embedding,[16] which minimizes the coupling between molecular vibrations and rotations away from equilibrium, it is desirable to employ this embedding in a large number of applications. However, the Eckart embedding leads to a complex analytical form of the rovibrational Hamiltonian even for a triatomic molecule;[21,22] consequently, to the best of our knowledge, no general polyatomic code employing internal coordinates exists which could perform rovibrational computations utilizing an Eckart frame. As shown here, the explicit knowledge of the kinetic energy operator can be circumvented and the numerical construction of the kinetic energy operator within the GENIUSH scheme results in a straightforward use of the Eckart embedding for arbitrary molecular systems.

In this work the embedding dependence and the range of applicability of the RRD scheme with respect to rotational excitation and rovibrational energy is investigated through numerical tests based on variational computations using curvilinear internal coordinates. In particular, rotational quantum labels are assigned to the rovibrational states of the $H_2{}^{16}O$ molecule via the RRD algorithm, using Jacobi coordinates either with the R_1 or bisector embeddings,[18] or employing valence coordinates (two OH bond lengths and the HOH bond angle) with the Eckart embedding.

II. THEORY OF RIGID ROTOR DECOMPOSITION

The following description of the RRD protocol follows closely that given in Ref. 13.

For a closed-shell molecule, in the absence of an external field and when neglecting hyperfine interactions, the J rotational quantum number is a good quantum number for the description of the overall molecular rotation; thus, the labeling of the nuclear motion states can be performed independently for different J values. Let us assume that the following three criteria are satisfied for an asymmetric-top molecule under investigation. (1) Given a J rotational quan-

tum number, the rovibrational time-independent Schrödinger equation $\hat{H}^{\text{rovib}}\Psi_n^{\text{rovib}} = E_n^{\text{rovib}}\Psi_n^{\text{rovib}}$, $n \in \{1, 2, \ldots, n_{\text{rovib}}\}$ is solved for n_{rovib} number of eigenpairs. Furthermore, the rovibrational E_n^{rovib} energy levels and Ψ_n^{rovib} wave functions (functions of the vibrational internal ccordinates and the rotational coordinates) are both available, but lack rovibrational quantum labels. (2) For the given J rotational quantum number, the rigid-rotor Schrödinger equation $\hat{H}^{\text{RR}}\Phi_n^{\text{RR}} = E_n^{\text{RR}}\Phi_n^{\text{RR}}$, $n \in \{1, 2, \ldots, 2J+1\}$ is also solved, providing $2J+1$ rotational wave functions for each vibrational state. These wave functions depend on the rotational coordinates, and each of them can be characterized by a unique set of rotational quantum labels. In the case of asymmetric tops, these quantum numbers are $\{J, K_a, K_c\}$, where J is the quantum number corresponding to the overall rotational motion of the molecule, while K_a and K_c correspond to the projections of the rotational angular momentum on the body-fixed z-axis for the prolate and oblate symmetric-top limits of the rigid rotor, respectively. (3) The $J = 0$ pure vibrational Schrödinger equation $\hat{H}^{\text{vib}}\psi_n^{\text{vib}} = E_n^{\text{vib}}\psi_n^{\text{vib}}$, $n \in \{1, 2, \ldots, n_{\text{vib}}\}$ is solved for n_{vib} eigenpairs. A unique vibrational label is assigned to each vibrational eigenstate, which could be obtained for low-energy states using the NMD protocol described in Ref. 13.

The RRD scheme is based on a $(2J+1) \cdot n_{\text{vib}}$-dimensional $|\psi_k^{\text{vib}}\Phi_l^{\text{RR}}\rangle = |\psi_k^{\text{vib}}\rangle \otimes |\Phi_l^{\text{RR}}\rangle$, $k \in \{1, 2, \ldots, n_{\text{vib}}\}, l \in \{1, 2, \ldots, 2J+1\}$, orthonormal, direct-product basis. As a result, each direct-product basis function has a unique rovibrational label.

The next step is the computation of the overlaps

$$S_{n;k,l} = \langle \Psi_n^{\text{rovib}} \mid \psi_k^{\text{vib}}\Phi_l^{\text{RR}}\rangle, \quad n \in \{1, 2, \ldots, n_{\text{rovib}}\},$$
$$k \in \{1, 2, \ldots, n_{\text{vib}}\}, \quad l \in \{1, 2, \ldots, 2J+1\}. \quad (1)$$

Then, for each Ψ_n^{rovib} the quantities $P_{n;k} = \sum_{l=1}^{2J+1} S_{n;k,l}^2$ are evaluated and collected into a table. These quantities are interpreted as the "total overlap" of the kth vibrational state and the nth rovibrational state. For each value of n, k_n^{max} is determined, $P_{n;k_n^{\text{max}}}$ being the largest of the $P_{n;k}$ values. Finally, Ψ_n^{rovib} is labeled with the rovibrational quantum numbers of the direct-product basis function with which its $S_{n;k_n^{\text{max}},l}$ overlap is the largest. Naturally, to obtain unique labels $(2J+1) \cdot n_{\text{vib}} \geq n_{\text{rovib}}$ must hold.

Besides providing unique quantum labels, determining the symmetry of the rovibrational states is also defined as a step in the RRD scheme. This can be done by determining the symmetry of the direct-product basis function which was used for the RRD labeling, which naturally has the same symmetry as the rovibrational state.

Since the $|\psi_k^{\text{vib}}\Phi_l^{\text{RR}}\rangle = |\psi_k^{\text{vib}}\rangle \otimes |\Phi_l^{\text{RR}}\rangle$, $k \in \{1, 2, \ldots, n_{\text{vib}}\}, l \in \{1, 2, \ldots, 2J+1\}$ direct-product functions span the rovibrational Hilbert space for a given J value, the $|\psi_k^{\text{vib}}\rangle \otimes |\Phi_l^{\text{RR}}\rangle$ direct-product functions transform among each other if operated on by a symmetry operator of the molecular symmetry (MS) group.[23] Let $|\psi^{\text{vib}}\rangle$ and $|\phi^{\text{RR}}\rangle$ be given variational vibrational and rigid-rotor eigenfunctions, respectively. If the symmetry of the $|\psi^{\text{vib}}\rangle$ and $|\phi^{\text{RR}}\rangle$ functions are known and they belong to a one-dimensional irreducible representation of the molecular point group (PG) and the molecular rotation group (RG), respectively, determining

the symmetry of $|\psi^{\text{vib}}\rangle \otimes |\phi^{\text{RR}}\rangle$ is straightforward. Let $\hat{R}_i^{\text{MS}}$, $\hat{R}_k^{\text{PG}}$, and $\hat{R}_l^{\text{RG}}$ denote the ith, kth, and lth symmetry operation of the MS, PG, and RG groups, respectively. If the $|\psi^{\text{vib}}\rangle$ and $|\phi^{\text{RR}}\rangle$ functions transform according to one-dimensional irreducible representations (assuming real character values), then $\hat{R}_k^{\text{PG}}|\psi^{\text{vib}}\rangle = \pm|\psi^{\text{vib}}\rangle$ and $\hat{R}_l^{\text{RG}}|\phi^{\text{RR}}\rangle = \pm|\phi^{\text{RR}}\rangle$. Thus, if the C_{kl}^i coefficients defined by $\hat{R}_i^{\text{MS}} = \sum_{k,l} C_{kl}^i \hat{R}_k^{\text{PG}} \hat{R}_l^{\text{RG}}$ are determined (for a given i all C_{kl}^i coefficients are zero, except one which equals to one, i.e., $C_{kl}^i = \delta_{kk_i'}\delta_{ll_i'}$), the expression $\hat{R}_i^{\text{MS}}|\psi^{\text{vib}}\phi^{\text{RR}}\rangle = \sum_{k,l} C_{kl}^i(\hat{R}_k^{\text{PG}}|\psi^{\text{vib}}\rangle \otimes \hat{R}_l^{\text{RG}}|\phi^{\text{RR}}\rangle)$ $= \hat{R}_{k_i'}^{\text{PG}}|\psi^{\text{vib}}\rangle \otimes \hat{R}_{l_i'}^{\text{RG}}|\phi^{\text{RR}}\rangle = \pm|\psi^{\text{vib}}\phi^{\text{RR}}\rangle$ can be evaluated, and $|\psi^{\text{vib}}\phi^{\text{RR}}\rangle$ can be labeled as a one-dimensional irreducible representation of the MS group. When the $|\psi^{\text{vib}}\rangle$ and $|\phi^{\text{RR}}\rangle$ functions transform according to multi-dimensional irreducible representations, the $\hat{R}_i^{\text{MS}}|\psi^{\text{vib}}\phi^{\text{RR}}\rangle$ functions will be linear combinations of the $|\psi_k^{\text{vib}}\Phi_l^{\text{RR}}\rangle$ functions; thus, determining the symmetry is not as simple and requires further considerations not discussed here.

III. ROVIBRATIONAL HAMILTONIANS

In this section we briefly describe the basics of rovibrational Hamiltonians related to our quantum chemical nuclear-motion approaches used for computing rotational-vibrational energies and wave functions variationally.

A. Embeddings

RRD overlaps $S_{n;k_n^{\text{max}},l}$ depend on the embedding of the molecule-fixed axis system chosen. Investigation of this dependence is one of the principal goals of the present study.

In this work RRD tables for the $H_2{}^{16}O$ molecule, chosen as our test system during all (ro)vibrational computations, are determined using the Jacobi (also known as scattering) coordinates with either the R_1 or bisector embeddings.[18] Although in the case of the bisector embedding the use of Radau coordinates seems to be a better choice for computing RRD overlaps, test computations show that RRD coefficients obtained with Radau coordinates are essentially identical with the ones obtained using Jacobi coordinates. Computations were also performed with valence internal coordinates and an Eckart embedding.[16] In the R_1 embedding (see Figure 1), the z-axis of the body-fixed frame is chosen to lie parallel to the interatomic vector described by the R_1 coordinate. In the bisector embedding, the x-axis of the body-fixed frame is chosen to bisect the angle between the interatomic R_1 vector and the R_2 vector connecting the center of mass of the diatom with the third atom. In the Eckart embedding, the body-fixed frame is chosen such that the nuclei satisfy the Eckart conditions.[16]

In order to make the body-fixed embeddings closer to the principal-axis system, in which the rigid-rotor computations were carried out, during the present study unorthodox choices were made for the R_1 and bisector embeddings (see Fig. 1). Within the R_1 embedding the molecule was placed in the (z,x)-plane with the body-fixed z-axis chosen to lie along the two H atoms, the x-axis "looking towards" the O atom in the plane of the molecule, and the y-axis chosen to give a right-handed coordinate system. In the bisector embedding the molecule
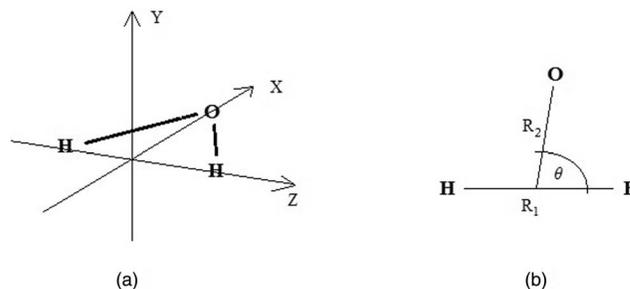

FIG. 1. Pictorial representation of (a) the R_1-embedding of the molecule in the body-fixed frame and (b) implementation of the Jacobi-coordinates in the R_1-embedding for the (ro)vibrational calculations.

was placed in the (z,x)-plane with the body fixed x-axis chosen to bisect the HOH bond angle in symmetric configurations.

In the case of the Eckart embedding the origin of the body-fixed frame was attached to the nuclear center of mass of the molecule. Thus, the three translational Eckart conditions are satisfied. There are two possible ways of maintaining the three rotational Eckart conditions. On one hand, the water molecule is to be placed into any of the three coordinate planes, thus two of the three rotational Eckart conditions are automatically statisfied. The third rotational Eckart condition can be maintained by rotating the nuclear position vectors by an angle given by Eq. (14) of Ref. 24. Alternatively, one can invoke the Eckart transformation method proposed in Ref. 25. The second method was favored in this study as it is general, while the first one applies only to triatomics.

B. Hamiltonians and their representation

The particular forms of the rovibrational Hamiltonians in the R_1 and bisector embeddings are taken from Refs. 26 and 27, respectively. To keep the discussion as brief as possible, the case of the R_1 embedding is discussed in detail in Sec. S.1 of the supplementary material,[28] while the case of the bisector embedding being essentially the same is omitted. For obtaining the matrix representation of the (ro)vibrational Hamiltonian in the R_1 and bisector embeddings, the D^2FOPI algorithm[26] was employed. Computations in the Eckart frame are based on a different approach, i.e., using the GENIUSH program suite which uses a fully numerical grid representation of the Hamiltonian. Interested readers should consult Refs. 19 and 20 for details on the GENIUSH protocol. Although the explicit form of the Hamiltonian in the Eckart embedding with Jacobi coordinates has been derived,[22] the fully numerical GENIUSH approach was chosen for these computations in order to take a more general and computationally more feasible route.

1. R_1 and bisector embeddings

The D^2FOPI (Ref. 26) approach utilizes an orthogonal and normalized product basis of the form $\{\chi_{n_1}(R_1)\chi_{n_2}(R_2)P_l^K(\cos\Theta)C_{MK}^{Jp}(\varphi,\chi,\psi)\}_{n_1=1,n_2=1,K=p,l=K}^{N_1,N_2,J,K+N_L-1}$, where the $\chi_{n_1}(R_1)$ and $\chi_{n_2}(R_2)$ functions are discrete variable representation (DVR) functions, $P_l^K(\cos\Theta)$ is the lth normalized associate Legendre function, $C_{MK}^{Jp}(\varphi,\chi,\psi)$ are

symmetry-adapted rotational functions of the form

$$C_{MK}^{Jp}(\varphi, \chi, \psi) = [2(1 + \delta_{K0})]^{-1/2} \left[D_{MK}^J + (-1)^p D_{M-K}^J \right],$$
$$p \in \{0, 1\}, \ K \in \{p, p+1, \ldots, J-1, J\}, \quad (2)$$

where p stands for parity,[29] M and K are the usual quantum numbers corresponding to space- and body-fixed projections of the rotational angular momentum on the appropriate z-axis, and D_{MK}^J are the normalized Wigner rotation functions.[29]

Due to the "almost" direct-product nature of the basis set (almost refers to the coupling between the $P_\ell^K(\cos \Theta)$ Legendre polynomials and the $C_{MK}^{Jp}(\varphi, \chi, \psi)$ rotation functions via K), the matrix representation of the triatomic Hamiltonian[18] can be written as a sum of direct product matrices, detailed in Sec. S.1 of the supplementary material.[28]

In order to have a compact basis expansion, in the R_1 and bisector computations $\chi_{n_1}(R_1)$ and $\chi_{n_2}(R_2)$ were chosen to be "potential optimized" (PO) DVR functions,[30–32] i.e., DVR functions obtained from the eigenfunctions of the 1D effective Hamiltonian $\hat{H}_j^{1D} = -\frac{1}{2\mu_j} \frac{d^2}{dR_j^2} + \hat{V}(R_j; R_{j'}, \Theta)$, $j, j' = 1, 2$ or $2, 1$ with $\hat{V}(R_j; R_{j'}, \Theta)$ chosen to be a relaxed 1D potential, i.e., $\hat{V}(R_j; R_{j'}, \Theta)$ is obtained by optimizing the $R_{j'}$ and Θ coordinates for each value of R_j, and μ_j is an appropriately defined mass-dependent constant.[26]

One can see from the formulae of Sec. S.1 of the supplementary material[28] that the matrix representation of the Hamiltonian has a very sparse and *a priori* known structure. This makes the use of an iterative eigensolver, e.g., the Lanczos algorithm[33–35] straightforward for obtaining the required eigenpairs.

The computation of rigid-rotor eigenpairs is performed by representing the rigid-rotor Hamiltonian on the same $C_{MK}^{Jp}(\varphi, \chi, \psi)$, $p \in \{0, 1\}$, $K \in \{p, p+1, \ldots, J-1, J\}$ rotational basis which was used for the rovibrational calculations in order to make the $S_{n;k,l} = \langle \Psi_n^{\mathrm{rovib}} | \psi_k^{\mathrm{vib}} \Phi_l^{\mathrm{RR}} \rangle$ RRD overlap computations straightforward. Details on the rigid-rotor computations are presented in Sec. S.2 of the supplementary material.[28]

2. Eckart embedding

The Eckart embedding[16] minimizes the coupling between molecular vibrations and rotations and is defined by three translational, $\sum_{i=1}^N m_i \mathbf{r}_i = \mathbf{0}$, and three rotational, $\sum_{i=1}^N m_i(\mathbf{r}_i \times \mathbf{R}_i) = \mathbf{0}$, conditions for a nonlinear molecule, where m_i, $\mathbf{r}_i$, and $\mathbf{R}_i$ stand for the nuclear masses, nuclear position vectors, and nuclear position vectors of the reference geometry of the Eckart frame, respectively.

To satisfy the three translational conditions the origin of the body-fixed frame needs to be shifted to the nuclear center of mass of the molecule. As a next step, the nuclear position vectors are to be rotated to the Eckart frame. The detailed description of this transformation for a general N-atomic molecule is given in Ref. 25 and thus it is not repeated here. However, in the special case of triatomics, two of the three rotational Eckart conditions are automatically satisfied if the molecule is placed to any of the three coordinate planes

of the body-fixed frame. The third condition can be maintained by a two-dimensional rotation with an angle given by Eq. (14) of Ref. 24. The first method, generally applicable for N-atomic molecules, has been implemented in the GENIUSH protocol. It is important to emphasize that the analytic form of the Eckart-embedded kinetic energy operator is not needed as the kinetic energy operator is represented numerically in the GENIUSH protocol.

IV. COMPUTATIONAL DETAILS

The test system chosen for the RRD analysis of the present study is the $H_2^{16}O$ isotopologue of the water molecule. The PES of Ref. 36 was employed in all nuclear motion computations. This choice facilitates comparison of the present results with those of the BT2 linelist.[37] Masses $m_O = 15.9994$ u and $m_H = 1.00794$ u were used throughout this study.

For the determination of the $J = 0$ (vibrational) and $J \neq 0$ (rovibrational) eigenpairs in the R_1 and bisector embeddings, the D^2FOPI program suite[26] was used. For the rigid-rotor computations the rotational constants were chosen, in cm^{-1}, as $A = 14.5964$, $B = 9.5274$, and $C = 27.4348$ when using the R_1 embedding, while $A = 9.5274$, $B = 14.5964$, and $C = 27.4348$ when using the bisector embedding. The same rotational constants are employed for all vibrational states. It appears to be natural to compute RRD overlaps using the vibrationally averaged rotational constants of each vibrational state. Our computations in the R_1 embedding for the $J = 15$ case show, however, that even a major change in the rotational constants, i.e., employing $A = 15.2770$, $B = 8.4600$, and $C = 73.0396$ which correspond to the (0 5 0) excited bending state, resulted in no change in the list of well-defined RRD labels.

When using the R_1 or bisector embeddings, the variational (ro)vibrational computations on the $H_2^{16}O$ molecule were performed employing (15, 20, 30) and (20, 25, 35) vibrational basis sets, respectively, whereby (n_1, n_2, n_p) means n_1 and n_2 PO spherical-DVR functions (with 300 primitive spherical functions) for the two distance-type and n_p Legendre basis functions for the angle-type coordinates. Naturally, a complete set of $2J + 1$ rotational basis functions was used in all cases. Following the notation of Ref. 26, the spherical oscillator basis functions of the R_1 and R_2 coordinates had parameters $R_1^{\max} = 4.6$ bohrs and $R_2^{\max} = 3.2$ bohrs, respectively.

When using the Eckart embedding via the GENIUSH protocol, valence coordinates (OH bond lengths r_1 and r_2, HOH bond angle Θ) were employed. The applied direct-product vibrational basis of size 12 000 consisted of 20 PO Hermite-DVR functions (with 80 primitive Hermite polynomials) for the two stretch coordinates and 30 Legendre-DVR functions for the bend coordinate. The GENIUSH computations utilized Wang combinations of the well-known symmetric top eigenfunctions as rotational basis functions.

V. EMBEDDING, ENERGY, AND *J* DEPENDENCE OF THE RRD SCHEME

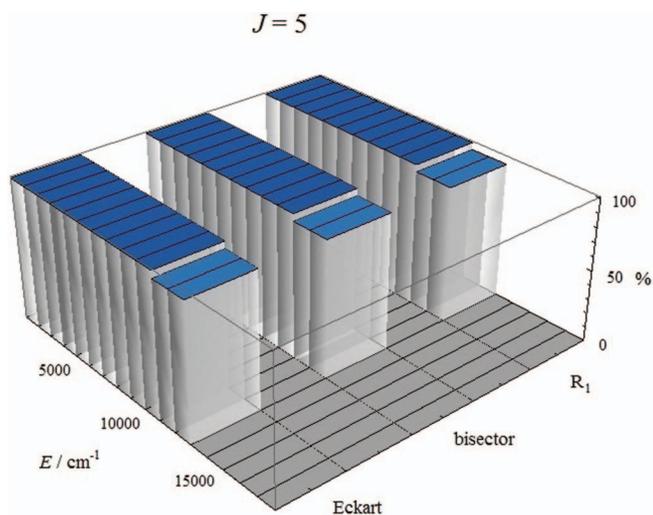Following the RRD scheme, rovibrational quantum labels were generated for the $H_2^{16}O$ molecule for all three

FIG. 2. Percentage of clearly assignable rovibrational states during the RRD analysis as a function of rovibrational energy in the R_1, bisector, and Eckart embeddings, for $J = 5$ rotational excitation.

FIG. 4. Percentage of clearly assignable rovibrational states during the RRD analysis as a function of rovibrational energy in the R_1, bisector, and Eckart embeddings, for $J = 15$ rotational excitation.

embeddings and for rotational quantum numbers $J = 5$, 10, and 15 for $30 \times (2J + 1)$ rovibrational eigenstates for each J. Vibrational normal-mode labels $(n_1\ n_2\ n_3)$ were taken from Ref. 10 by matching energies, which is straightforward for the vibrational states investigated, while the rotational asymmetric top limit $J_{K_a K_c}$ labels were generated during the rigid-rotor computations following the standard rigid-rotor labeling scheme.[29]

In terms of rovibrational states being the linear combination of the direct-product functions obtained from vibrational and rigid-rotor eigenfunctions, rovibrational states become more "mixed" with increasing energy and J rotational quantum number. This naturally leads to less dominant RRD overlaps [see Eq. (1)]. Figures 2–4 show the percentage of clearly assignable rovibrational states as a function of rovibrational energy for $J = 5$, 10, and 15, respectively. Each figure includes results for all three embeddings. RRD labels were
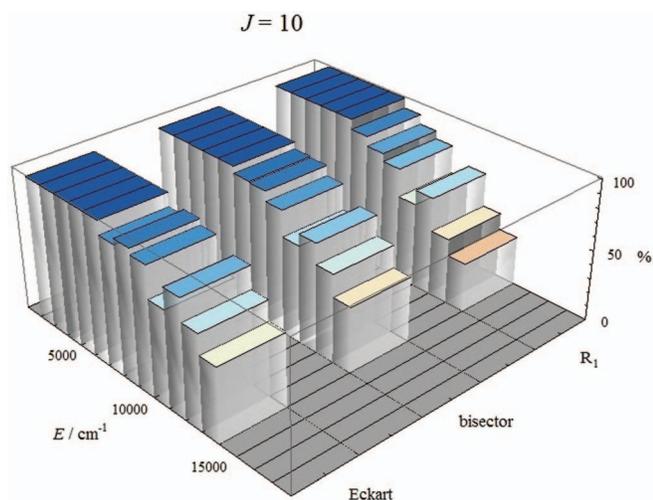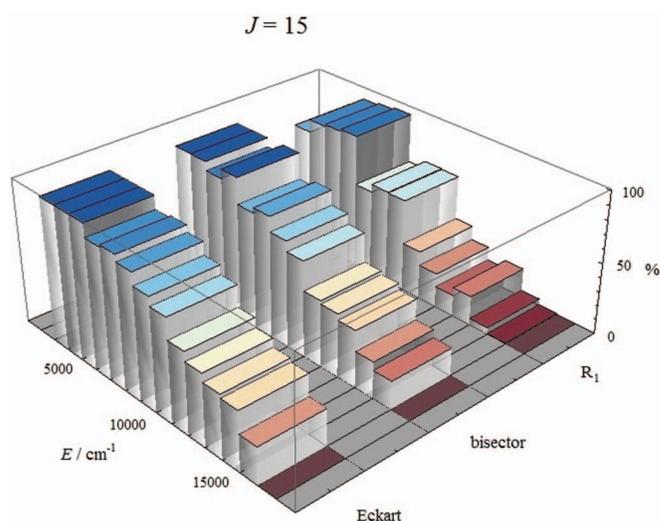
considered "well defined" if for the given rovibrational state the square of the largest $S_{n;k_n^{\max},l}$ coefficient from Eq. (1) exceeded 0.5, as suggested by the Hose–Taylor theorem.[38] As expected, less and less RRD labels are "well defined" with increasing energy and J quantum number. Nonetheless, for a wide range of both of these parameters a large number of "well defined" labels can be assigned via the RRD protocol. Out of the total of 1865 states included in Figs. 2–4, 973, 1211, and 1288 states could be given a "well defined" status when using the R_1, bisector, and Eckart embeddings, respectively.

It is noted that the choice of 0.5 as a lower limit for the square of the largest $S_{n;k_n^{\max},l}$ coefficients for considering a RRD label "well defined" is not the only possible one. With a lower threshold, one could extend the range of applicability of the RRD scheme considerably; however, this may lead to embedding-dependent quantum labels and in a few cases to duplicate labels. For example, choosing a cut-off value of 0.33, we obtain 1368, 1566, and 1596 well-defined labels for the R_1, bisector, and Eckart embeddings, respectively, but out of these 10, 17, and 25 are assigned twice and in 21 cases the assigned RRD labels are embedding dependent, i.e., the assigned labels differ in the different embeddings.

Another strategy is to consider a RRD label well defined if the second largest $S_{n;k_n^{\max},l}$ overlap is smaller than some portion of the largest $S_{n;k_n^{\max},l}$ overlap. Although with this method the number of well-defined labels can be increased, it leads, unfortunately, to some duplicate labels. Curing this problem needs special attention and the procedure cannot be automated.

As emphasized already in Ref. 13 and seen clearly in Figs. 2–4, the RRD coefficients depend on the embedding used for the rovibrational computations. Naturally, one expects and indeed experiences the least RRD "mixing" when the coupling between the rotational and vibrational coordinates is minimal, i.e., in the Eckart embedding. The Eckart embedding is clearly the best choice especially at the lowest

FIG. 3. Percentage of clearly assignable rovibrational states during the RRD analysis as a function of rovibrational energy in the R_1, bisector, and Eckart embeddings, for $J = 10$ rotational excitation.
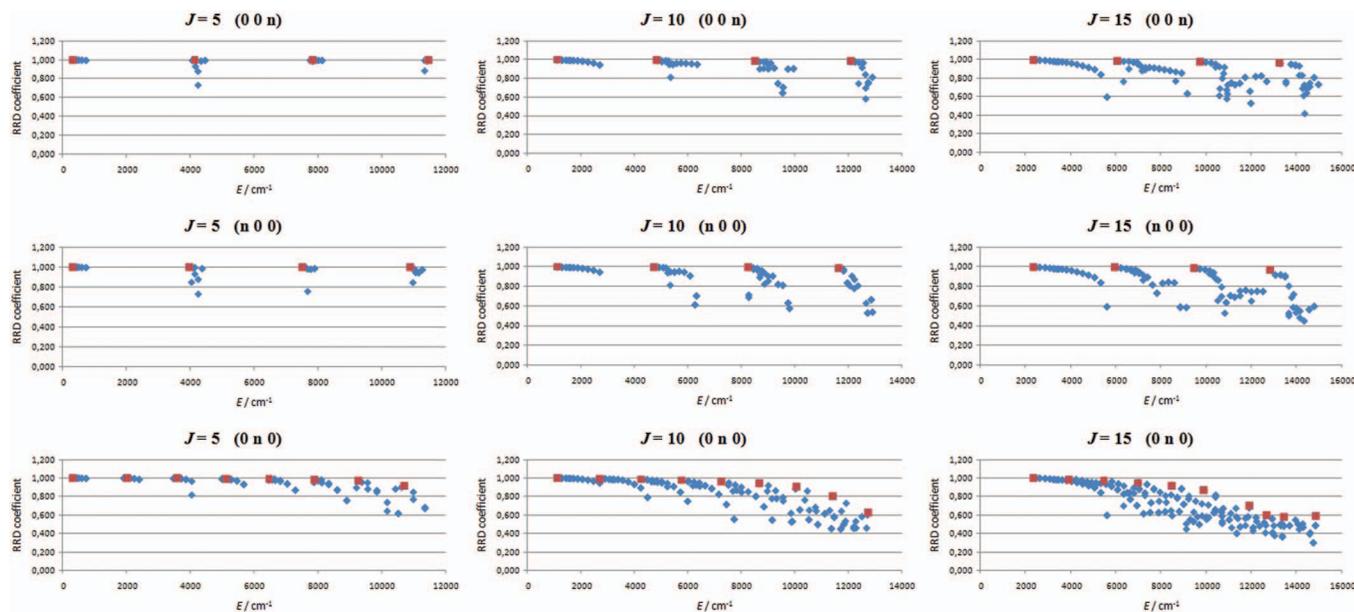
FIG. 5. The largest RRD coefficients obtained in the Eckart embedding as a function of rovibrational energy. $(n\ 0\ 0)$, $(0\ 0\ n)$, and $(0\ n\ 0)$ refer to approximate vibrational quantum labels for symmetric stretch, antisymmetric stretch, and bend, respectively. In all these cases the states included in the given plot have vibrational quantum labels such that all normal modes but the one excited by n quanta are in their ground state. Blue rectangles stand for rovibrational states, while red squares depict rovibrational states with the largest RRD overlap within a given vibrational manifold.

end of the spectrum. Although the Eckart embedding minimizes the coupling between molecular vibrations and rotations, Fig. 4 shows the "breakdown" of the Eckart embedding farther away from the equilibrium structure. At higher energies and rotational excitation rovibrational coupling is considerable even in the Eckart embedding, which is represented by the small maximum RRD coefficient values in such spectral regions. For the computation of rovibrational eigenstates an embedding different from the Eckart one might be more efficient. In a given application, one has to find a balance between computational efficiency and "mixing" of the RRD coefficients and choose the embedding accordingly.

Finally, the relation between monodromy[39–42] and assigning RRD labels is examined. Quantum monodromy,[43] which leads to a change in the energy level structure when a bent molecule starts to sample linear geometries, was discussed for the $H_2{}^{16}O$ water isotopologue in Ref. 44. As noted by Zobov *et al.*,[44] "*monodromy in quantum mechanical systems implies the absence of a single, smoothly varying set of quantum numbers with which to characterize the system.*" Monodromy could explain the breakdown of the RRD protocol when high excitation of the bending mode is involved. Rovibrational states for the $H_2{}^{16}O$ molecule with assigned vibrational labels including excitations for only a single normal mode were included in Fig. 5 to compare the energy dependence of the $S_{n;k_n^{max},l}$ overlap values for rovibrational states with different types of vibrational excitation. Inspecting the red squares in Fig. 5, standing for rovibrational states with the largest $S_{n;k_n^{max},l}$ overlap within a given vibrational state, one can observe that states with pure bending excitations [plots with $(0\ n\ 0)$] show a breakdown in the $S_{n;k_n^{max},l}$ overlaps from around 10 000 cm^{-1}, close to the barrier to linearity of water.[45–47] Thus, it seems that monodromy might at least partially explain the breakdown of the RRD protocol for rovibra-

tional states with high bending excitation. Such a breakdown is not observable for the symmetric $(n\ 0\ 0)$ and antisymmetric $(0\ 0\ n)$ stretching states. Nevertheless, as the n and J values increase the stretching states also start exhibiting smaller and smaller maximum RRD coefficients.

VI. COMPARISON WITH BT2 LABELS

One of the linelists available for $H_2{}^{16}O$ is the so-called BT2 linelist.[37] Comparing the "well defined" rovibrational labels of $H_2{}^{16}O$ obtained from the RRD in the Eckart embedding with the labels found in the BT2 linelist one can observe and appreciate the usefulness of the RRD labeling protocol.

Based on this comparison, one might divide the calculated rovibrational states into five groups: (a) rovibrational states which are assigned both in the BT2 linelist and during the RRD and have the same labels in the two cases, (b) states which are assigned both in the BT2 and during the RRD but have different labels in the two cases, (c) states which are assigned during the RRD but have no assignment in the BT2, (d) states which have an assigned label in the BT2 linelist but are not assigned during the RRD, and finally (e) states which are not assigned in either the BT2 or during the RRD. In Fig. 6 rovibrational states of $H_2{}^{16}O$ are separated according to their (a)-(e) type and are marked on the figure based on their energy.

As expected, for lower-energy states both the RRD scheme and the protocol employed when generating the BT2 linelist provide assigned labels which are in excellent agreement. It is only at around 5500 cm^{-1} that a few states start to show "mixing" in the RRD and thus cease to be "well defined."

The few dozen cases where both BT2 and RRD have assigned but different labels need special attention and need to
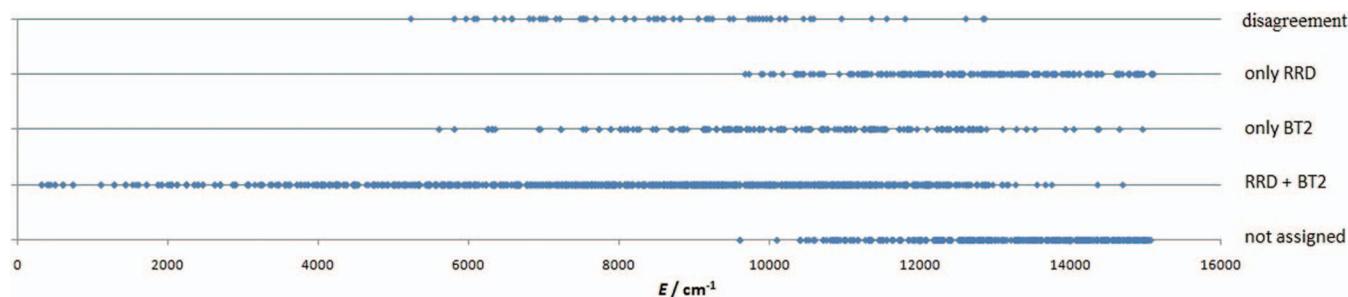
FIG. 6. $J = 5$, $J = 10$, and $J = 15$ rovibrational states of $H_2{}^{16}O$ separated according to their (a)-(e) type (see Sec. VI) and marked on the figure based on their energy.

be examined individually. The RRD scheme is thus useful not only to provide labels for yet unassigned states but also to verify existing labels.

The usefulness of the RRD scheme can especially be appreciated from about 10 000 cm^{-1}, where the BT2 linelist starts lacking assigned labels. From around 10 000 cm^{-1} up to around 15 000 cm^{-1}, there are many states which lack BT2 labels, but can be assigned via the RRD scheme.

The number of states lacking RRD labels, as seen in Fig. 6, naturally increases with energy. One might notice that from around 10 000 cm^{-1} states lacking any assignment start appearing quite suddenly. The explanation of this behavior may again involve arguments based on quantum monodromy.[44]

VII. SUMMARY AND CONCLUSIONS

In the fourth age of quantum chemistry[5] codes implementing the variational solution of the time-independent nuclear-motion Schrödinger equation become more and more standard tools of theoretical molecular spectroscopy. Assigning exact and approximate quantum numbers to the large collection of computed eigenstates is important to turn data into knowledge, solve chemically significant problems, and develop self-consistent spectroscopic databases built upon spectroscopic networks.[48,49]

In this work the original[13] RRD scheme developed with respect to the Eckart–Watson Hamiltonian has been extended to work with Hamiltonians written in terms of internal coordinates using either the R_1, the bisector, or the Eckart embeddings. The RRD coefficients are still defined by projecting rotational-vibrational wave functions onto products of rigid-rotor basis functions and previously determined vibrational eigenstates. The rotational label of the rovibrational eigenstate is selected based on the largest overlap in a row of the RRD table.

As one would expect, numerical comparison of RRD overlaps for $H_2{}^{16}O$ in the different embeddings shows the superiority of the Eckart embedding, i.e., Eckart-based RRD overlaps exhibit less mixing than those corresponding to the other embeddings. The bisector embedding performs slightly better than the R_1 embedding, at least for the water molecule.

Irrespective of the embedding employed, the RRD tables yield unambiguous labels for the overwhelming majority of the eigenstates corresponding to the lower-energy end of the spectrum. However, the RRD scheme starts breaking down at higher excitation energies and for higher J values. Numerical results clearly show that the RRD scheme provides considerably more unambiguous labels for rotations than the NMD scheme is able to do for vibrations. This suggests that the rigid-rotor approximation holds better for rotations than the normal-mode approximation for vibrations.

Based on Fig. 6, several labels in the BT2 linelist[37] of $H_2{}^{16}O$ might be problematic, since they disagree with clear assignments obtained from the RRD protocol. This aspect of the present study will be explored in more detail.

[1] P. F. Bernath, Phys. Chem. Chem. Phys. **4**, 1501 (2002).
[2] J. Tennyson, "Accurate variational calculations for line lists to model the vibration-rotation spectra of hot astrophysical atmospheres," Wiley Interdiscip. Rev.: Comput. Mol. Sci. (to be published).
[3] J. Tennyson, P. F. Bernath, L. R. Brown, A. Campargue, M. R. Carleer, A. G. Császár, R. R. Gamache, J. T. Hodges, A. Jenouvrier, O. V. Naumenko, O. L. Polyansky, L. S. Rothman, R. A. Toth, A. C. Vandaele, N. F. Zobov, L. Daumont, A. Z. Fazliev, T. Furtenbacher, I. F. Gordon, S. N. Mikhailenko, and S. V. Shirin, J. Quant, J. Quant. Spectrosc. Radiat. Transf. **110**, 573 (2009).
[4] J. Tennyson, P. F. Bernath, L. R. Brown, A. Campargue, A. G. Császár, L. Daumont, R. R. Gamache, J. T. Hodges, O. V. Naumenko, O. L. Polyansky, L. S. Rothman, R. A. Toth, A. C. Vandaele, N. F. Zobov, S. Fally, A. Z. Fazliev, T. Furtenbacher, I. F. Gordon, S.-M. Hu, S. N. Mikhailenko, and B. Voronin, J. Quant. Spectrosc. Radiat. Transf. **111**, 2160 (2010).
[5] A. G. Császár, C. Fábri, T. Szidarovszky, E. Mátyus, T. Furtenbacher, and G. Czakó, Phys. Chem. Chem. Phys. **14**, 1085 (2012).
[6] S. N. Yurchenko, W. Thiel, and P. Jensen, J. Mol. Spectrosc. **245**, 126 (2007).
[7] J. M. Bowman, T. Carrington, and H.-D. Meyer, Mol. Phys. **106**, 2145 (2008).
[8] C. Fábri, E. Mátyus, T. Furtenbacher, B. Mihály, T. Zoltáni, L. Nemes, and A. G. Császár, J. Chem. Phys. **135**, 094307 (2011).
[9] T. Carrington, in *Encyclopedia of Computational Chemistry*, edited by P. v. R. Schleyer, N. L. Allinger, T. Clark, J. Gasteiger, P. A. Kollman, H. F. Schaefer III, and P. R. Schreiner (Wiley, Chichester, 1998), Vol. 5, pp. 3157–3166.

[10]A. G. Császár, E. Mátyus, T. Szidarovszky, L. Lodi, N. F. Zobov, S. V. Shirin, O. L. Polyansky, and J. Tennyson, J. Quant. Spectrosc. Radiat. Transf. **111**, 1043 (2010).

[11]B. C. Silva, P. Barletta, J. J. Munro, and J. Tennyson, J. Chem. Phys. **128**, 244312 (2008).

[12]N. F. Zobov, S. V. Shirin, L. Lodi, B. C. Silva, J. Tennyson, A. G. Császár, and O. L. Polyansky, Chem. Phys. Lett. **507**, 48 (2011).

[13]E. Mátyus, C. Fábri, T. Szidarovszky, G. Czakó, W. D. Allen, and A. G. Császár, J. Chem. Phys. **133**, 034113 (2010).

[14]P. R. Schreiner, H. P. Reisenauer, E. Mátyus, A. G. Császár, A. Siddiqi, A. C. Simmonett, and W. D. Allen, Phys. Chem. Chem. Phys. **11**, 10385 (2009).

[15]D. A. Sadovskii, N. G. Fulton, J. R. Henderson, J. Tennyson, and B. I. Zhilinskii, J. Chem. Phys. **99**, 906 (1993).

[16]C. Eckart, Phys. Rev. **47**, 552 (1935).

[17]J. K. G. Watson, Mol. Phys. **15**, 479 (1968).

[18]B. T. Sutcliffe and J. Tennyson, Int. J. Quantum Chem. **39**, 183 (1991).

[19]E. Mátyus, G. Czakó, and A. G. Császár, J. Chem. Phys. **130**, 134112 (2009).

[20]C. Fábri, E. Mátyus, and A. G. Császár, J. Chem. Phys. **134**, 074105 (2011).

[21]H. Wei and T. Carrington, Jr., Chem. Phys. Lett. **287**, 289 (1998).

[22]H. Wei and T. Carrington, Jr., J. Chem. Phys. **107**, 2813 (1997).

[23]P. R. Bunker and P. Jensen, *Molecular Symmetry and Spectroscopy*, 2nd ed. (NRC Research Press, Ottawa, 1998).

[24]C. R. Le Sueur, S. Miller, J. Tennyson, and B. T. Sutcliffe, Mol. Phys. **76**, 1147 (1992).

[25]A. Y. Dymarsky and K. N. Kudin, J. Chem. Phys. **122**, 124103 (2005).

[26]T. Szidarovszky, A. G. Császár, and G. Czakó, Phys. Chem. Chem. Phys. **12**, 8373 (2010).

[27]J. Tennyson and B. T. Sutcliffe, Int. J. Quantum Chem. **42**, 941 (1992).

[28]See supplementary material at http://dx.doi.org/10.1063/1.4707463 for the Hamiltonian matrix elements in the R_1 embedding and the rigid-rotor Hamiltonian and its matrix representation.

[29]R. N. Zare, *Angular Momentum* (Wiley, New York, 1988).

[30]H. Wei and T. Carrington, Jr., J. Chem. Phys. **97**, 3029 (1992).

[31]J. Echave and D. C. Clary, Chem. Phys. Lett. **190**, 225 (1992).

[32]V. Szalay, G. Czakó, Á. Nagy, T. Furtenbacher, and A. G. Császár, J. Chem. Phys. **119**, 10512 (2003).

[33]C. Lanczos, J. Res. Natl. Bur. Stand. **45**, 255 (1950).

[34]J. K. Cullum and R. A. Willoughby, *Lanczos Algorithms for Large Symmetric Eigenvalue Computations* (Birkhauser, Boston, 1985).

[35]Y. Saad, *Iterative Methods for Sparse Linear Systems* (Society for Industrial and Applied Mathematics (SIAM), Philadelphia, 2003).

[36]S. V. Shirin, O. L. Polyansky, N. F. Zobov, P. Barletta, and J. Tennyson, J. Chem. Phys. **118**, 2124 (2003).

[37]R. J. Barber, J. Tennyson, G. J. Harris, and R. N. Tolchenov, Mon. Not. R. Astron. Soc. **368**, 1087 (2006).

[38]G. Hose and H. S. Taylor, Phys. Rev. Lett. **51**, 947 (1983).

[39]M. Hazewinkel, *Encyclopaedia of Mathematics* (Reidel/Kluwer, 1994).

[40]J. E. Marsden and M. J. Hoffman, *Basic Complex Analysis* (Freeman, New York, 1987).

[41]R. Cushman, Centruumvoor Wiskund Inf. Newslett. **1**, 4 (1983).

[42]L. R. Bates, J. Appl. Math. Phys. **42**, 837 (1991).

[43]M. S. Child, T. Weston, and J. Tennyson, Mol. Phys. **96**, 371 (1999).

[44]N. F. Zobov, S. V. Shirin, O. L. Polyansky, J. Tennyson, P.-F. Coheur, P. F. Bernath, M. Carleer, and R. Colin, Chem. Phys. Lett. **414**, 193 (2005).

[45]A. G. Császár, W. D. Allen, and H. F. Schaefer III, J. Chem. Phys. **108**, 9751 (1998).

[46]G. Tarczay, A. G. Császár, W. Klopper, V. Szalay, W. D. Allen, and H. F. Schaefer III, J. Chem. Phys. **110**, 11971 (1999).

[47]E. F. Valeev, W. D. Allen, H. F. Schaefer III, and A. G. Császár, J. Chem. Phys. **114**, 2875 (2001).

[48]T. Furtenbacher, A. G. Császár, and J. Tennyson, J. Mol. Spectrosc. **245**, 115 (2007).

[49]A. G. Császár and T. Furtenbacher, J. Mol. Spectrosc. **266**, 99 (2011).